







Optical O₂ Sensors Also Respond to Redox Active Molecules Commonly Secreted by Bacteria

 Avi I. Flamholz,^{a,b}  Samuel Saccomano,^c  Kevin Cash,^{c,d}  Dianne K. Newman^{a,b,e}

^aDivision of Biology and Biological Engineering, California Institute of Technology, Pasadena, California, USA

^bResnick Sustainability Institute, California Institute of Technology, Pasadena, California, USA

^cChemical and Biological Engineering, Colorado School of Mines, Golden, Colorado, USA

^dQuantitative Biosciences and Engineering, Colorado School of Mines, Golden, Colorado, USA

^eDivision of Geological and Planetary Sciences, California Institute of Technology, Pasadena, California, USA

ABSTRACT From a metabolic perspective, molecular oxygen (O₂) is arguably the most significant constituent of Earth's atmosphere. Nearly every facet of microbial physiology is sensitive to the presence and concentration of O₂, which is the most favorable terminal electron acceptor used by organisms and also a dangerously reactive oxidant. As O₂ has such sweeping implications for physiology, researchers have developed diverse approaches to measure O₂ concentrations in natural and laboratory settings. Recent improvements to phosphorescent O₂ sensors piqued our interest due to the promise of optical measurement of spatiotemporal O₂ dynamics. However, we found that our preferred bacterial model, *Pseudomonas aeruginosa* PA14, secretes more than one molecule that quenches such sensors, complicating O₂ measurements in PA14 cultures and biofilms. Assaying supernatants from cultures of 9 bacterial species demonstrated that this phenotype is common: all supernatants quenched a soluble O₂ probe substantially. Phosphorescent O₂ probes are often embedded in solid support for protection, but an embedded probe called O₂NS was quenched by most supernatants as well. Measurements using pure compounds indicated that quenching is due to interactions with redox-active small molecules, including phenazines and flavins. Uncharged and weakly polar molecules like pyocyanin were especially potent quenchers of O₂NS. These findings underscore that optical O₂ measurements made in the presence of bacteria should be carefully controlled to ensure that O₂, and not bacterial secretions, is measured, and motivate the design of custom O₂ probes for specific organisms to circumvent sensitivity to redox-active metabolites.

IMPORTANCE When they are closely packed, as in biofilms, colonies, and soils, microbes can consume O₂ faster than it diffuses. As such, O₂ concentrations in natural environments can vary greatly over time and space, even on the micrometer scale. Wetting soil, for example, slows O₂ diffusion higher in the soil column, which, in concert with microbial respiration, greatly diminishes [O₂] at depth. Given that variation in [O₂] has outsized implications for microbial physiology, there is great interest in measuring the dynamics of [O₂] in microbial cultures and biofilms. We demonstrate that certain classes of bacterial metabolites frustrate optical measurement of [O₂] with phosphorescent sensors, but also that some species (e.g., *E. coli*) do not produce problematic secretions under the conditions tested. Our work therefore offers a strategy for identifying organisms and culture conditions in which optical quantification of spatiotemporal [O₂] dynamics with current sensors is feasible.

KEYWORDS *Pseudomonas aeruginosa*, oxygen, pyocyanin, redox-active metabolites, sensors

The O₂/H₂O redox couple ($E^{\circ} \approx +800$ mV) is the most favorable terminal electron acceptor used by biology. Indeed, aerobic microbes typically regulate their metabolisms to use O₂ before any other terminal acceptor (1), even those with very favorable midpoint potentials like

Editor Deborah A. Hogan, Geisel School of Medicine at Dartmouth

Copyright © 2022 Flamholz et al. This is an open-access article distributed under the terms of the [Creative Commons Attribution 4.0 International license](https://creativecommons.org/licenses/by/4.0/).

Address correspondence to Dianne K. Newman, dkn@caltech.edu.

The authors declare no conflict of interest.

Received 5 August 2022

Accepted 7 October 2022

Published 31 October 2022

nitrate ($\text{NO}_3^- \rightarrow \text{NO}_2^-$, $E^\circ \approx +370$ mV). Today, O₂ is abundantly produced by photosynthetic organisms, leading to an atmospheric partial pressure of $\approx 21\%$ and equilibrium aqueous concentrations of $\approx 200\text{--}400$ μM (2). This enormous reservoir of oxidant powers the complex multicellular organisms and vibrant ecosystems living near Earth's surface.

Yet a wide variety of natural environments, ranging from soils to the insides of animals, are characterized by very low O₂ concentrations ($[\text{O}_2]$). Organisms endemic to such environments are termed "functional anaerobes" as they often rely on enzymes that are irreversibly deactivated by oxygen and cannot grow in high O₂ settings. This toxicity is due to the reactivity of O₂ itself as well as reactive oxygen species (e.g., H₂O₂ and O₂⁻) that are produced from O₂ through biotic and abiotic mechanisms (3). O₂-impacted physiology also matters practically: low O₂ correlates with antibiotic tolerance (4).

Microbiologists typically categorize environments as "oxic," "anoxic," or "hypoxic," but natural environments are heterogeneous and often characterized by intermediate and fluctuating O₂ levels. Along the murine intestinal tract, for example, $[\text{O}_2]$ can range from subambient in the stomach (≈ 50 μM) to near anoxia (< 1 μM) in cecum (5). This difference is consequential: microbes express alternative respiratory pathways when $[\text{O}_2]$ is depleted (1). Similarly, intestinal O₂ levels decrease substantially when respiratory metabolism is stimulated by addition of glucose (6), so the O₂ level that microbes experience depends on the balance of inflow and local metabolism.

When they are densely packed in environments like biofilms, colonies, or soils, microbes can consume O₂ faster than it diffuses, generating suboxic microenvironments that affect metabolism and growth (7). Spatial transcriptomic data suggest that such microenvironments induce large changes in gene expression (8). We might intuit that microbes tune their gene expression, metabolism, and physiology in response to the local environment, yet bacterial gene expression is noisy (9) and often imperfectly optimized for growth and survival even in batch culture (10). We would like to understand how bacteria adapt to communal life in spatially heterogeneous settings, but our inability to measure the chemical microenvironment limits our capacity to interpret the "omics" data already collected.

Given its centrality to metabolism and physiology, there is great interest in measuring $[\text{O}_2]$ in natural environments (11) and laboratory experiments (12–15). Bulk O₂ concentrations can be measured via several methods (16). However, few of these approaches can measure spatiotemporal O₂ dynamics to characterize chemical microenvironments (11, 17, 18). Planar optodes are constructed by coating a surface with a phosphorescent O₂-sensing dye over which a semipermeable polymer matrix is applied as insulation. As O₂ quenches dye phosphorescence, the optode can be calibrated by measuring phosphorescence intensity or lifetime in known O₂ concentrations (17, 19).

In principle, these dyes could be used in solution to measure $[\text{O}_2]$ at high spatiotemporal resolution. However, O₂-sensing dyes are also quenched by molecules other than O₂ (20). This problem has motivated engineering of sensors protected from spurious interactions by chemical modification (20, 21) or polymer encapsulation (5, 13). Impressed by recent measurements of spatiotemporal O₂ dynamics in rodent brains (21) and intestines (5), we attempted similar measurements in *Pseudomonas aeruginosa* (PA14) biofilms. As PA14 is known for its secretion of many small molecules, including redox-active phenazines (22), we first tested whether culture supernatants quench a model soluble O₂ sensor, RTDP (17, 23).

We grew PA14 in a minimal medium where it reliably produces the phenazine pyocyanin (PYO) and found that RTDP was strongly quenched by filtered supernatants. Undiluted supernatants reduced fluorescence by $\approx 50\%$ (Fig. 1B and Fig. S2), similar to ambient levels of O₂ (24). Quenching of RTDP by organics is well-documented (23) and could be due to several chemical mechanisms (25). We therefore proceeded to test a "protected" sensor, O₂NS, composed of an O₂-sensitive platinum-bound porphyrin encapsulated in a spherical ≈ 200 nm PVC matrix (13). Neat PA14 supernatants appeared to quench O₂NS fluorescence by $\approx 40\%$ (Fig. S3). We quantified the concentration-dependence of quenching as an effective Stern-Volmer constant K_{SV} (19); larger values indicate greater quenching (Fig. 1C and D).

Photochemical electron transfer is one mechanism by which small molecules quench phosphorescence (25). We therefore hypothesized that quenching is due to secretion of

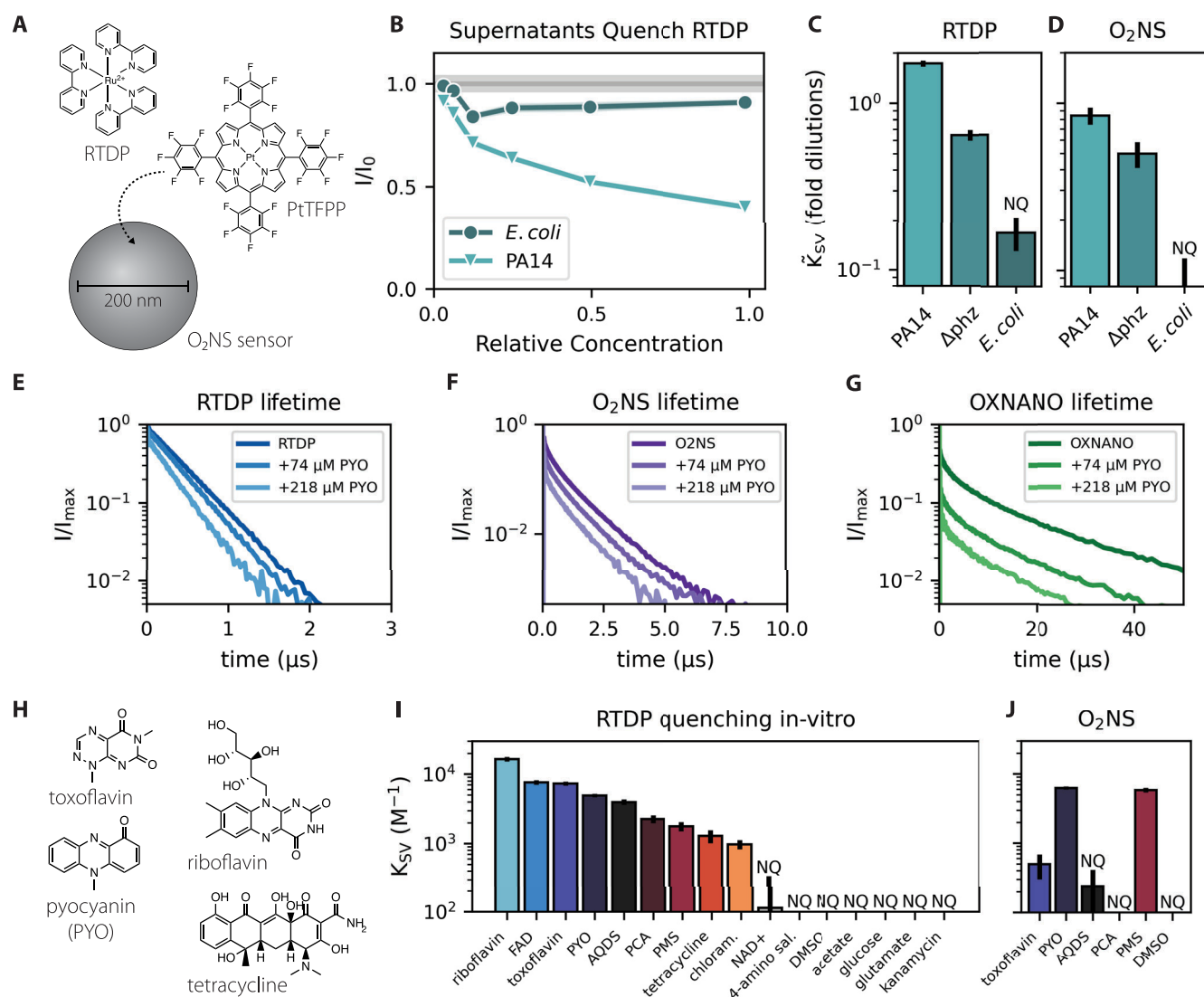


FIG 1 Bacteria secrete soluble quenchers of phosphorescent O₂ sensors. (A) Tris(2,2'-bipyridyl)dichlororuthenium(II), or RTDP, is a soluble phosphorescent ruthenium complex that can be used as an O₂ sensor (17). Platinum (II) meso-tetra(pentafluorophenyl)porphine, or PtTFPP, is the O₂-sensing component of O₂NS nanosensors, which encapsulate the Pt-porphyrin with a reference dye in a spherical ≈200 nm PVC matrix (13). (B) Strains were grown in a minimal medium where *P. aeruginosa* (PA14) reliably produces pyocyanin (26). Serially diluted PA14 supernatants quenched RTDP in a concentration-dependent manner. I/I₀ denotes fluorescence normalized to no quencher, and the width of the horizontal gray bar gives the standard deviation of RTDP intensity in culture media. (C–D) Quantification shows that PA14 supernatants quench RTDP and O₂NS, and that quenching is partially due to secreted phenazines. The concentration-dependence of quenching was fit to a Stern-Volmer model (19) where $I/I_0 = (1 + \bar{K}_{SV}[Q])^{-1}$. Quencher concentration [Q] has units of (fold dilutions)⁻¹ here. $\bar{K}_{SV} = 1$ implies I/I₀ = 0.5 when [Q] = 1, i.e., for an undiluted supernatant; larger \bar{K}_{SV} imply stronger quenching. Deletion of phenazine biosynthesis genes (PA14 Δphz) reduced but did not eliminate quenching, and *E. coli* supernatants quenched both sensors far less than PA14. (E–G) Phosphorescence lifetime measurements of RTDP, O₂NS and a commercial O₂ sensor, OXNANO, indicated that the phenazine pyocyanin (PYO) is a strong concentration-dependent quencher of all three sensors. Panels give normalized intensities (I/I_{max}). (H) A subset of biological molecules tested for RTDP quenching. Panel (I) gives the results of serial dilution measurements akin to panel B. Here, K_{SV} has M⁻¹ units. Redox active molecules capable of spontaneous electron transfer were stronger quenchers. (J) O₂NS was quenched by many of the same molecules, but encapsulation appears to protect against quenching by polar and charged species like toxoflavin and PCA. Error bars mark a 95% confidence interval. “NQ” denotes “nonquencher” where the fit to a Stern-Volmer model was poor or quenching was too weak to quantify (Fig. S1). Abbreviations: flavin adenine dinucleotide (FAD), 9,10-Anthraquinone 2,6-disulfonic acid (AQDS), phenazine 1-carboxylic acid (PCA), phenazine methosulphate (PMS), chloramphenicol (chloram.), NAD (NAD+), 4-amino salicylate (4-amino sal.), dimethyl sulfoxide (DMSO).

redox-active molecules like phenazines, which is common in *Pseudomonas* species (22). Consistent with this hypothesis, supernatants from a strain lacking phenazine biosynthesis (PA14 Δphz) grew to similar densities as wild-type, but quenched RTDP and O₂NS to a lesser extent (Fig. 1C and D, Fig. S3 and S4). Nonetheless, PA14 Δphz supernatants still quenched both sensors substantially more than *E. coli* supernatants, with fit PA14 Δphz \bar{K}_{SV} being ≈4-fold larger for RTDP and ≈8-fold larger for O₂NS. Accordingly, we conclude that PA14 secretes more than one class of molecules that quench phosphorescent O₂ sensors.

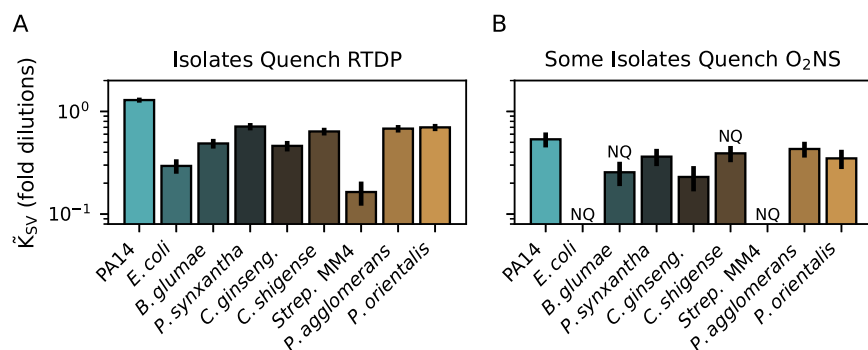


FIG 2 Bacteria commonly secrete soluble quenchers of phosphorescent O₂ sensors. (A) Supernatants from 7 additional bacterial strains were screened for RTDP quenching activity after growth in a glucose minimal medium supplemented with amino acids. All supernatants quenched RTDP measurably, but to various degrees. (B) Screened supernatants quenched O₂NS to a lesser extent. Error bars give 95% confidence intervals. “NQ” denotes “nonquencher” where the fit to a Stern-Volmer model was poor or quenching was too weak to quantify (Fig. S1). Strains are described in Table S1.

As PA14 makes substantial PYO in our minimal medium (26), we used lifetime spectroscopy to verify that PYO quenches three distinct phosphorescent O₂ sensors *in vitro*: RTDP, O₂NS, and a commercial sensor called OXNANO (Fig. 1E–G). We next tested a variety of small molecules with diverse biological functions in a serial dilution assay. Redox-active molecules quenched RTDP while controls lacking spontaneous redox activity did not (Fig. 1I and Fig. S5). As these serial dilution experiments were conducted on the benchtop, we assumed that redox active molecules were predominantly oxidized.

We then assayed O₂NS with a subset of the molecules considered in Fig. 1I. Despite large RTDP quenching constants, molecules carrying net charge at neutral pH (PCA, AQDS) did not quench O₂NS and were not differentiable from the negative control, DMSO (Fig. 1J and Fig. S6). This likely reflects the low solubility of charged molecules in the hydrophobic PVC matrix of O₂NS particles. In contrast, PYO and PMS, which are uncharged and have little polar surface area, quenched O₂NS and RTDP with large associated K_{SV} values. Toxoflavin is uncharged but has a relatively larger polar surface area, which may explain its ≈ 15 -fold lower K_{SV} for O₂NS.

To understand whether bacteria commonly secrete quenchers of phosphorescent O₂ sensors, we tested supernatants from 7 additional bacterial species selected based on their ability to grow in our minimal medium supplemented with amino acids. All supernatants quenched RTDP measurably (Fig. 2A and Fig. S7). O₂NS was also quenched by several culture supernatants, but less strongly than RTDP (Fig. 2B and Fig. S8). Despite the change in growth media, *E. coli* supernatants did not quench O₂NS.

Conclusions. Motivated by the need to measure chemical microenvironments to better understand microbial physiology at the microscale, we attempted to make optical measurements of O₂ dynamics in the presence of bacterial secretions. We found that model phosphorescent O₂ sensors were substantially quenched by supernatants from several bacterial species (Fig. 1). Quenchers in *P. aeruginosa* PA14 supernatants included, but were not limited to, phenazines (Fig. 1B and C). Encapsulating the O₂-sensitive molecule in a protective matrix, as in O₂NS, reduced quenching but did not eliminate it in most cases (Fig. 1D and F). *In vitro* experiments indicated that quenching was due to interactions with redox-active secreted molecules like pyocyanin (Fig. 2). Indeed, the pyocyanin concentration can surpass 100 μ M in PA14 supernatants (22); such concentrations quenched O₂NS by $\approx 40\%$, comparable to ≈ 30 μ M O₂ (13). Several published works report optical O₂ quantifications using similar sensors in the presence of growing bacteria (12–15). Such measurements typically rely on calibration curves measured in the absence of cells (12, 13, 15), or in the presence of unknown concentrations of bacterial secretions (14). Our results indicate that additional controls are required to demonstrate that the bacteria under study do not produce spurious quenchers in the chosen culture conditions.

With some exceptions (24), RTDP is not usually used to measure [O₂] in the presence of living cells, likely due to the potential for spurious quenching. Rather, we used RTDP to demonstrate that microbes commonly secrete quenchers (Fig. 1D) and intended the

RTDP-O₂NS comparison to illustrate the protective effect of the polymer matrix, which is substantial (Fig. 1D and E) but depends on quencher chemistry (Fig. 2C and Fig. S8). These results indicate that diverse bacteria secrete small-molecule quenchers that are likely redox-active (Fig. 1I). We therefore suggest that RTDP might be used to identify copious producers like PA14. Notably, *E. coli* supernatants did not quench O₂NS (Fig. 1C and E), indicating that O₂NS and similar sensors might succeed in measuring spatiotemporal [O₂] dynamics in the presence of growing *E. coli* cells. Our protocol for using serial dilutions to estimate supernatant quenching (Methods and Fig. S1) therefore offers a road-map for identifying mutually compatible organisms, growth media, and O₂ sensors for optical characterization of the chemical microenvironment. Toward the goal of mapping spatiotemporal variation in O₂ concentrations in diverse systems, our work spotlights the opportunity and need to design O₂ sensors appropriate for specific applications.

Strains and culture conditions. All strains were grown in a glucose minimal medium (GMM) comprising 10 mM glucose 50 mM KH₂PO₄/K₂HPO₄ (pH 7.2), 42.8 mM NaCl, 9.35 mM NH₄Cl, 1 mM MgSO₄, and a trace elements solution. The medium was prepared by autoclaving all the components together, except for the glucose and the 1000× trace elements stock solution, which were sterilized through filtration and added after autoclaving (26). For the experiments reported in Fig. 1E and F, 1× MEM Amino Acids solution (MilliporeSigma, Cat. No. M5550) was added so that diverse strains could be grown in the same media. For experiments focused on fast-growing strains (Fig. 1A to D) strains were pre-grown to saturation in 5 mL GMM (≈24 h) and back-diluted by adding 200 μL saturating culture to 5 mL fresh GMM. Experimental cultures were grown for 24 h before collecting supernatants (see below). For experiments, including slower-growing strains (Fig. 1E and F) precultures were grown for ≈60 h, back-diluted and allowed to grow 48 h before collecting supernatants. Bacterial strains are described in Table S1.

Chemical stocks. Pyocyanin (PYO) was synthesized from phenazine methosulphate (PMS) as described previously (26) and a 7.5 mM stock was prepared in 20 mM HCl. Unless otherwise noted, other chemical stocks were prepared at 10 mM in a filter-sterilized 25 mM HEPES buffer (pH 7) and stored at 4°C between experiments. The following chemicals were sourced from Sigma-Aldrich: NAD⁺ (β-NAD hydrate, N1511), FAD (flavin adenine dinucleotide disodium salt hydrate, F6625), riboflavin (R-4500), L-glutamic acid monosodium salt hydrate (G1626-100G), sodium 4-aminosalicylate dihydrate (A-3505) and tetracycline (T-3383). 1 M d-glucose (Alfa Aesar A16828) and acetate (sodium acetate trihydrate; Fischer Scientific S209-500) were prepared in milliQ water and diluted to 10 mM in buffer. PMS (Alfa Aesar, H56718) stocks were prepared fresh due to its known photoconversion to PYO. Toxoflavin (MedChemExpress) was dissolved in dimethyl sulfoxide (DMSO, Macron Fine Chemicals) to make a 10 mM stock solution (26). Lab stocks of kanamycin sulfate (Gibco 11815-024, 103 mM in water) and chloramphenicol (Sigma C0378, 77.3 mM in ethanol) were diluted to 10 mM in HEPES buffer. 500× RTDP (100 mg/mL Tris(2,2'-bipyridyl)dichlororuthenium(II) hexahydrate, Sigma-Aldrich 544981) stocks were prepared in milliQ water. Multiple O₂NS batches were prepared on the same date as previously reported (13) and pooled into a single stock that was used for all experiments.

Measurement of supernatant quenching by serial dilution. Cultures supernatants were collected by centrifugation of 1 to 2 mL of saturating culture (6 min. at 5,000g) in a benchtop centrifuge (Eppendorf 5418). Five hundred μL of culture supernatant was filtered through 0.22 μm sterile spin filters (Costar Spin-X, Cat. No. 8160), which were centrifuged for 2 min. at 10,000g. Filtered supernatants were then 2-fold serially diluted 3 to 5 times in 100 μL volume in a 96-well plate (BRANDplates 781671). Wells containing 100 μL of fresh culture media were included as blanks. Optical measurements were then conducted using a Tecan Spark 10 M plate reader. Absorbance spectra were recorded to verify dilution and fluorescence measurements were taken to quantify the baseline (“preaddition”) fluorescence of each supernatant. RTDP was excited at 450 nm and fluorescence was monitored at 625 nm; for O₂NS experiments, both dyes were excited at 450 nm, PtFPP was monitored at 650 nm and DiA 585 nm (13). After baseline measurements, the appropriate sensor (RTDP or O₂NS) was added to all wells and fluorescence was measured again (“postaddition”). For O₂NS, 11 μL stock was added to each well after which well contents were mixed by pipetting and 11 μL was withdrawn to conserve the total volume. In early experiments (Fig. 1A to D), 1 μL of

100× RTDP was added to each well. In later experiments (Fig. 1E and F) 11 μ L of 10× RTDP was added and withdrawn as described for O₂NS samples. Culture densities were recorded in 5× dilution at 500 nm (Beckman Coulter DU 800). Strains were grown in biological duplicate and each supernatant was assayed in technical duplicate. The procedure for fitting effective quenching constants (K_{SV}) from these data are described below.

Measurement of pure chemical quenching by serial dilution. Stocks of pure chemicals were diluted to a defined concentration and then 2-fold serially diluted five times in 100 μ L volume in a 96-well plate (BRANDplates 781671). The starting concentrations were as follows: 10 mM acetate and glucose, 500 μ M 4-amino salicylate, AQDS, FAD, glutamate, NAD⁺, PCA, PMS, tetracycline and toxoflavin, 502.5 μ M chloramphenicol and PYO, 504.7 μ M kanamycin, and 200 μ M riboflavin. Wells containing 100 μ L of buffer were included as blanks. Optical measurements were conducted in a Tecan Spark 10 M plate reader as described above, i.e., first recording baseline absorbance spectra and fluorescence levels and then recording fluorescence again after sensor addition (RTDP or O₂NS). This procedure is diagrammed in Fig. S1. Excitation and emission parameters are given above. The procedure for fitting quenching constants (K_{SV}) is described below.

Fitting quenching constants from serial dilution experiments. The Stern-Volmer plots in Fig. S2 and 3 and S5 to 8 plot sensor I_0/I against quencher concentration [Q]. The Stern-Volmer equation predicts a linear relationship of $I_0/I = 1 + K_{SV} [Q]$. I_0 is sensor fluorescence intensity in the absence of any quencher (i.e., in buffer), which was quantified from the postaddition fluorescence of control wells. Since the supernatants and pure chemicals used were often fluorescent, sensor fluorescence in the presence of quencher (I) was calculated from the dilution series by subtracting the rescaled baseline measurement from the postaddition fluorescence. Rescaling was necessary because the preaddition sample was typically diluted by $\approx 10\%$ by the addition of the sensor in order to maintain a constant sample volume and path-length. For a 10% dilution, then, $I = I_{\text{post}} - 0.9 I_{\text{pre}}$. As 11 μ L was added to a 100 μ L in most experiments, actual dilution factors were $(1 - 11/111) \approx 0.9$. Given this $\approx 10\%$ dilution, quencher concentrations were also rescaled before generating Stern-Volmer plots and fitting quenching constants. That is, $[Q] = [Q_{\text{pre}}] * 0.9$ for the example of 10% dilution. We then used weighted linear least-squares fitting (Python statsmodels package) to fit I_0/I to a linear function of [Q]. Data points were weighted by estimated accuracy (1/variance) inferred by error propagation through blanking and ratio calculation. The slope of this fit was taken to be K_{SV} . Symmetric 95% confidence intervals on K_{SV} were calculated using the same package. As inner filter effects can be confused with quenching, we omitted the highest concentration of intrinsically fluorescent molecules (e.g., PYO, PMS, AQDS) from the K_{SV} fit. Chemicals and supernatants were marked "NQ" for "nonquencher" if [Q] was poorly correlated with I_0/I (Pearson $R < 0.4$) or if the magnitude of quenching overlapped with the variability measured for the unquenched sensor. This analysis pipeline is diagrammed in Fig. S1. All source code for data processing and figure generation can be found at github.com/flamholz/secretions_quench_o2sensors.

Phosphorescence lifetime measurements. All lifetime measurements were conducted in a 25 mM HEPES buffer (pH 7.0). Buffer was air-equilibrated by bubbling house air for 1 h. RTDP stock was diluted to 40 μ M for measurement and O₂NS was diluted 10-fold from stock. A 0.5 mg/mL stock of OXNANO (PyroScience) was prepared and then diluted 10-fold into aerated HEPES buffer for measurement. All measurements were conducted in a custom-built lifetime fluorometer in the Caltech Beckman Institute Laser Resource Center. Lifetimes were first measured in 2 mL volumes in quartz cuvettes without PYO to choose measurement parameters and establish a baseline lifetime. All sensors were excited at 355 nm; RTDP and O₂NS were monitored at 650 nm, OXNANO at 750 nm. PYO stock (7.5 mM) was then added to the cuvette in defined volumes—2 μ L, 18 μ L, 20 μ L, 20 μ L—and lifetimes were measured between additions. Cuvettes were stirred by a magnetic stir-bar during measurement.

SUPPLEMENTAL MATERIAL

Supplemental material is available online only.

FIG S1, PDF file, 0.8 MB.

FIG S2, PDF file, 0.04 MB.

FIG S3, PDF file, 0.04 MB.

FIG S4, PDF file, 0.02 MB.

FIG S5, PDF file, 0.1 MB.

FIG S6, PDF file, 0.03 MB.

FIG S7, PDF file, 0.04 MB.

FIG S8, PDF file, 0.04 MB.

TABLE S1, XLSX file, 0.01 MB.

ACKNOWLEDGMENTS

Thanks to Chelsey VanDrise for supplying pyocyanin, Andrew Babbin for OXNANO beads, Lucas Meirelles and John Ciemniecki for assistance with toxoflavin and *B. glumae* cultivation. Thanks to Josh Goldford, Darcy McRose, Georgia Squyers, Lev Tsy-pin, and Shuangning Xu for useful conversations. This investigation was aided by a Postdoctoral Fellowship from The Jane Coffin Childs Memorial Fund for Medical Research (to A.I.F.) and NIH grants (1R01AI127850-01A1 and 1R01HL152190-01) to D.K.N. as well as the US Department of Energy (DOE) Office of Science, Office of Biological and Environmental Research Bioimaging Science Program under subcontract B643823 (to K.C.) and the LLNL 3DQ Microscope Project, SCW1713.

REFERENCES

- Körner H, Zumft WG. 1989. Expression of denitrification enzymes in response to the dissolved oxygen level and respiratory substrate in continuous culture of *Pseudomonas stutzeri*. *Appl Environ Microbiol* 55:1670–1676. <https://doi.org/10.1128/aem.55.7.1670-1676.1989>.
- Milo R, Phillips R. 2015. *Cell Biology by the Numbers*. Garland Science. <https://market.android.com/details?id=book-9NPRCgAAQBAJ>.
- Lu Z, Imlay JA. 2021. When anaerobes encounter oxygen: mechanisms of oxygen toxicity, tolerance and defence. *Nat Rev Microbiol* 19:774–785. <https://doi.org/10.1038/s41579-021-00583-y>.
- Borriello G, Werner E, Roe F, Kim AM, Ehrlich GD, Stewart PS. 2004. Oxygen limitation contributes to antibiotic tolerance of *Pseudomonas aeruginosa* in biofilms. *Antimicrob Agents Chemother* 48:2659–2664. <https://doi.org/10.1128/AAC.48.7.2659-2664.2004>.
- Friedman ES, Bittinger K, Espipova TV, Hou L, Chau L, Jiang J, Mesaros C, Lund PJ, Liang X, FitzGerald GA, Goulian M, Lee D, Garcia BA, Blair IA, Vinogradov SA, Wu GD. 2018. Microbes vs. chemistry in the origin of the anaerobic gut lumen. *Proc Natl Acad Sci U S A* 115:4170–4175. <https://doi.org/10.1073/pnas.1718635115>.
- Bohlen HG. 1980. Intestinal tissue PO₂ and microvascular responses during glucose exposure. *Am J Physiol* 238:H164–71. <https://doi.org/10.1152/ajpheart.1980.238.2.H164>.
- Keilluweit M, Wanzek T, Kleber M, Nico P, Fendorf S. 2017. Anaerobic microsites have an unaccounted role in soil carbon stabilization. *Nat Commun* 8:1–10. <https://doi.org/10.1038/s41467-017-01406-6>.
- Dar D, Dar N, Cai L, Newman DK. 2021. Spatial transcriptomics of planktonic and sessile bacterial populations at single-cell resolution. *Science* 373:1–16. <https://doi.org/10.1126/science.abi4882>.
- Elowitz MB, Levine AJ, Siggia ED, Swain PS. 2002. Stochastic gene expression in a single cell. *Science* 297:1183–1186. <https://doi.org/10.1126/science.1070919>.
- LaCroix RA, Sandberg TE, O'Brien EJ, Utrilla J, Ebrahim A, Guzman GI, Szubin R, Palsson BO, Feist AM. 2015. Use of adaptive laboratory evolution to discover key mutations enabling rapid growth of *Escherichia coli* K-12 MG1655 on glucose minimal medium. *Appl Environ Microbiol* 81:17–30. <https://doi.org/10.1128/AEM.02246-14>.
- Tengberg A, Hovdenes J, Andersson HJ, Brocandel O, Diaz R, Hebert D, Americh T, Huber C, Körtzinger A, Khripounoff A, Rey F, Rönning C, Schimanski J, Sommer S, Stanglmayer A. 2006. Evaluation of a lifetime-based optode to measure oxygen in aquatic systems. *Limnol Oceanogr Methods* 4:7–17. <https://doi.org/10.4319/lom.2006.4.7>.
- Ladner T, Flitsch D, Schlepütz T, Büchs J. 2015. Online monitoring of dissolved oxygen tension in microtiter plates based on infrared fluorescent oxygen-sensitive nanoparticles. *Microb Cell Fact* 14:1–14. <https://doi.org/10.1186/s12934-015-0347-9>.
- Jewell MP, Galyean AA, Kirk Harris J, Zemanick ET, Cash KJ. 2019. Luminescent Nanosensors for Ratiometric Monitoring of Three-Dimensional Oxygen Gradients in Laboratory and Clinical *Pseudomonas aeruginosa* Biofilms. *Appl Environ Microbiol* 85:1–12. <https://doi.org/10.1128/AEM.01116-19>.
- Smriga S, Ciccarese D, Babbin AR. 2021. Denitrifying bacteria respond to and shape microscale gradients within particulate matrices. *Commun Biol* 4:1–9. <https://doi.org/10.1038/s42003-021-02102-4>.
- Jusková P, Schmitt S, Kling A, Rackus DG, Held M, Egli A, Dittrich PS. 2021. Real-Time Respiration Changes as a Viability Indicator for Rapid Antibiotic Susceptibility Testing in a Microfluidic Chamber Array. *ACS Sens* 6:2202–2210. <https://doi.org/10.1021/acssensors.1c00020>.
- Berg JS, Ahmerkamp S, Pjevac P, Hausmann B, Milucka J, Kuypers MMM. 2022. How low can they go? Aerobic respiration by microorganisms under apparent anoxia. *FEMS Microbiol Rev* 46:1–14. <https://doi.org/10.1093/femsre/fuac006>.
- Wolfbeis OS, Weis LJ, Leiner MJP, Ziegler WE. 1988. Fiber-optic fluorosensor for oxygen and carbon dioxide. *Anal Chem* 60:2028–2030. <https://doi.org/10.1021/ac00170a009>.
- Wang X-D, Wolfbeis OS. 2014. Optical methods for sensing and imaging oxygen: materials, spectroscopies and applications. *Chem Soc Rev* 43:3666–3761. <https://doi.org/10.1039/c4cs00039k>.
- Gehlen MH. 2020. The centenary of the Stern-Volmer equation of fluorescence quenching: from the single line plot to the SV quenching map. *J Photochem Photobiol C: Photochem Rev* 42:100338. <https://doi.org/10.1016/j.jphotochemrev.2019.100338>.
- Esipova TV, Karagodov A, Miller J, Wilson DF, Busch TM, Vinogradov SA. 2011. Two new “protected” oxyphors for biological oximetry: properties and application in tumor imaging. *Anal Chem* 83:8756–8765. <https://doi.org/10.1021/ac2022234>.
- Esipova TV, Barrett MJP, Erlebach E, Masunov AE, Weber B, Vinogradov SA. 2019. Oxyphor 2P: a high-performance probe for deep-tissue longitudinal oxygen imaging. *Cell Metab* 29:736–744. <https://doi.org/10.1016/j.cmet.2018.12.022>.
- Glasser NR, Saunders SH, Newman DK. 2017. The colorful world of extracellular electron shuttles. *Annu Rev Microbiol* 71:731–751. <https://doi.org/10.1146/annurev-micro-090816-093913>.
- Kalyanasundaram K. 1982. Photophysics, photochemistry and solar energy conversion with tris(bipyridyl)ruthenium(II) and its analogues. *Coord Chem Rev* 46:159–244. [https://doi.org/10.1016/0010-8545\(82\)85003-0](https://doi.org/10.1016/0010-8545(82)85003-0).
- Gerritsen HC, Sanders R, Draaijer A, Ince C, Levine YK. 1997. Fluorescence lifetime imaging of oxygen in living cells. *J Fluoresc* 7:11–15. <https://doi.org/10.1007/BF02764572>.
- Balzani V, Ceroni P, Juris A. 2014. *Photochemistry and photophysics: concepts, research, applications*. John Wiley & Sons. <https://play.google.com/store/books/details?id=TKw6AwAAQBAJ>.
- Meirelles LA, Newman DK. 2022. Phenazines and toxoflavin act as interspecies modulators of resilience to diverse antibiotics. *Mol Microbiol* . <https://doi.org/10.1111/mmi.14915>.